Transverse beam size measurement system using visible synchrotron radiation at HLS II *

Kai Tang(唐凯)[1] Bao-Gen Sun(孙葆根)[2] Yong-Liang Yang(杨永良) Ping Lu(卢平)
Lei-Lei Tang(唐雷雷) Fang-Fang Wu(吴芳芳) Chao-Cai Cheng(程超才)
Jia-Jun Zheng (郑佳俊) Hao Li (李浩)
National Synchrotron Radiation Laboratory, University of Science and Technology of China, Hefei 230029, China

Abstract: An interferometer system and an imaging system using visible synchrotron radiation (SR) have been installed in the Hefei Light Source (HLS) II storage ring. Simulations of these two systems are given using Synchrotron Radiation Workshop (SRW) code. With these two systems, the beam energy spread and the beam emittance can be measured. A detailed description of these two systems and the measurement method is given in this paper. The measurement results of beam size, emittance and energy spread are given at the end.

Keywords: HLS II, interferometer, beam profile, beam energy spread, beam emittance

PACS: 29.20.db, 29.85.Ca, 29.90.+r **DOI:** 10.1088/1674-1137/40/9/097002

1 Introduction

Visible synchrotron radiation (SR) has been widely used for electron beam diagnostics in storage rings. Overviews of transverse beam profile diagnostics based on emitted SR have been given by Kube [1] and Takano [2] respectively. Beam diagnostic methods based on SR can be classified as imaging methods, exploitation of SR wave-optics features (such as π-polarization), projection methods and interference methods [3]. The measurement resolution is limited in a simple imaging system (using visual SR) due to diffraction effects [1]. However, a simple imaging system was still applied at beamline B8 of the Hefei Light Source (HLS) II [4] because the imaging system can monitor the beam state directly. HLS II is a second generation SR source with several hundred μm transverse beam size both horizontally and vertically.

An SR interferometer was first applied to measure the beam size by Mitsuhashi at the ATF damping ring [5–8]. Now it has become a universal tool and has been applied in numerous facilities [9−18]. T. Naito and T. Mitsuhashi applied an interferometer with Herschelian reflective optics to reduce dispersion effects of the objective lens. By this method, the interferometer can measure a 4.7 μm beam size [19]. P. Chevtsov utilized an interferometer to measure the beam energy spread by ignoring the intrinsic beam size [9]. At HLS II, an interferometer system has been installed at beamline B7 and a simple imaging system at beamline B8 [4, 20].

With knowledge of the machine optical parameters and relative energy spread, the emittance can be inferred from the measured beam size [1]. Usually, the beam energy is not a constant and depends on beam current. So emittance is not a direct value. The two source point technique to measure emittance and energy spread simultaneously was performed at ALS [21, 22]. In this paper, we give a detailed description of the measurement of these two quantities in combination with the imaging system and the interferometer system at HLS II.

The measurement method of the beam energy spread and the horizontal beam emittance using these two systems is described in Section 2.1. The configurations of these two systems are described in Section 2.2. The simulation results computed by SRW [23] are given in 2.3. The measured results are given in Section 3.

2 Experimental methods

2.1 Measurement theory

The theory of beam size measurement with interferometers is well-documented. It is a wavefront division two-beam interferometer using polarized quasi-monochromatic light. The SR wavefront is divided by a double slit and merged again at the image plane. Taking the vertical channel as an example, the fringe distribu-

Received 26 February 2016, Revised 25 April 2016
∗ Supported by National Natural Science Foundation of China (11105141, 11175173) and Upgrade Project of Hefei Light Source
1) E-mail: tangkkai@mail.ustc.edu.cn
2) E-mail: bgsun@mail.ustc.edu.cn

tion [7] at the image plane is described by:

$$I(y)=I_0\mathrm{sinc}^2\left(\frac{\pi w_y}{\lambda L'}y\right)\left(1+\gamma_y\cos\left(\frac{2\pi d_y}{\lambda L'}y+\phi_0\right)\right), \quad (1)$$

where w_y denotes the vertical size of the slit, L' denotes the distance between the double slits and the detector, d_y denotes the separation of the two slits, λ denotes the wavelength, ϕ_0 denotes the fringe phase, and γ_y denotes the complex degree of coherence. If the beam shape is a Gaussian profile [11], γ_y is given by:

$$\gamma_y=\exp\left\{-2\left(\frac{\pi d_y\sigma_y}{\lambda L}\right)^2\right\}, \quad (2)$$

where σ_y denotes the beam size. Inverting Eq. (2):

$$\sigma_y=\frac{\lambda L}{\pi d_y}\sqrt{\frac{1}{2}\ln\frac{1}{\gamma_y}}. \quad (3)$$

At HLS II, the fringe was fitted by the following function:

$$I(y)=a_1\mathrm{sinc}^2(a_2(y-a_5))\{1+a_3\cos[a_4(y-a_6)]\}+a_7, \quad (4)$$

where sinc denotes the $\sin(x)/x$ function, $a_1, a_2, ..., a_7$ are fitting parameters, and a_3 is γ_y.

The theory of transverse beam size measurement with the imaging system is simple. Ideally, the intensity profile monitored by the camera would correspond to the beam profile at the source point scaled by the magnification factor of the system [15]. By integrating the raw data along the x direction and y direction respectively, two curves can be achieved. The beam size can be directly inferred by fitting these curves with a Gaussian function:

$$I(x)=a_1\exp\left(-\frac{(x-a_2)^2}{2{a_3}^2}\right)+a_4 \quad (5)$$

where a_1 is related to light intensity, a_2 is the peak position of the curve and is related to beam position, a_3 is the beam size, and a_4 is related to the camera noise. The beam size is inferred by dividing a_3 by a magnification ratio. This fitting model takes account of the camera noise and the background from stray illumination. The offset must be taken into account to fit the profile with the Gaussian function.

Usually, the horizontal beam size has two sources: the portion due to betatron oscillation and the portion due to dispersion. Let ε_x denote horizontal beam emittance and δ denote relative energy spread.

$$\varepsilon_x=\frac{\sigma_x^2-\delta^2\eta_x^2}{\beta_x}, \quad (6)$$

where β_x is a betatron function and η is a dispersion function. By subtracting the part due to dispersion, the beam emittance can be inferred. Let $\sigma_\beta=\sqrt{\varepsilon_x\beta_x}$ denote the size due to betatron oscillation and $\sigma_\delta=\delta\eta$ denote the size due to dispersion. For the B8 source point, σ_β (178.9 μm) can be compared to σ_δ (131.3 μm). For the B7 source point, σ_δ (49.8 μm) is far less than σ_β (247.4 μm).

For the storage ring, the beam emittance and energy spread do not depend on the longitudinal position. Thus, horizontal beam emittance and energy spread at the B7 and B8 source point are the same. They can be described by:

$$\begin{cases}{\sigma_{x,1}}^2=\varepsilon_x\beta_{x,1}+\delta^2{\eta_{x,1}}^2\\{\sigma_{x,2}}^2=\varepsilon_x\beta_{x,2}+\delta^2{\eta_{x,2}}^2\end{cases} \quad (7)$$

where subscript 1 represents B7 and subscript 2 represents B8. We can solve for ε_x and δ from Eq. (7):

$$\begin{cases}\varepsilon_x=({\sigma_{x,1}}^2{\eta_{x,2}}^2-{\sigma_{x,2}}^2{\eta_{x,2}}^2)/(\beta_{x,1}{\eta_{x,2}}^2-\beta_{x,2}{\eta_{x,1}}^2)\\\delta=[({\sigma_{x,2}}^2\beta_{x,1}-{\sigma_{x,1}}^2\beta_{x,2})/(\beta_{x,1}{\eta_{x,2}}^2-\beta_{x,2}{\eta_{x,1}}^2)]^{1/2}\end{cases} \quad (8)$$

By measuring the horizontal beam sizes at the B7 and B8 source points simultaneously, the horizontal beam emittance and the beam energy spread can be inferred from Eq. (8).

2.2 Experimental setup

HLS II is a second generation electron storage ring with an electron energy of 800 MeV. It has fourfold periodicity with a total of eight 45° sector magnets, a circumference of 66 m, a design transverse beam emittance of 36.4 nm.rad and a design relative energy spread of 4.7×10^{-4}. Table 1 lists the beam parameters and the theoretical beam sizes at the B7 and B8 source points.

Table 1. Optics parameters and beam size at the B7 and B8 source points.

parameters	B7	B8
β_x/m	1.7668	0.9235
β_y/m	12.3485	7.6854
η_x/m	0.1059	0.2793
η'_x	−0.1990	−0.4754
design transverse ε/(nm·rad)	36.4	
design energy spread δ	4.7×10^{-4}	
σ_x/μm with 10% coupling	246.9	218.6
σ_y/μm with 10% coupling	202.1	159.5

Figure 1 shows the schematic layout of the interferometer system. The SR is reflected 90° downwards by an oxygen-free copper mirror (mirror 1) in the vacuum chamber. After being reflected by mirror 2 and mirror 3, the SR is transmitted to an optical table. On the optical table, the SR light is divided by a splitter (splitter 1). The SR of these two channels passes through a double slit, an achromatic lens with 1000 mm focal length, another lens (lens 2) with 100 mm focal length, a polarizer

and a 500 nm bandpass filter. The image is observed by a Procilica GE680 camera which is placed at the image plane.

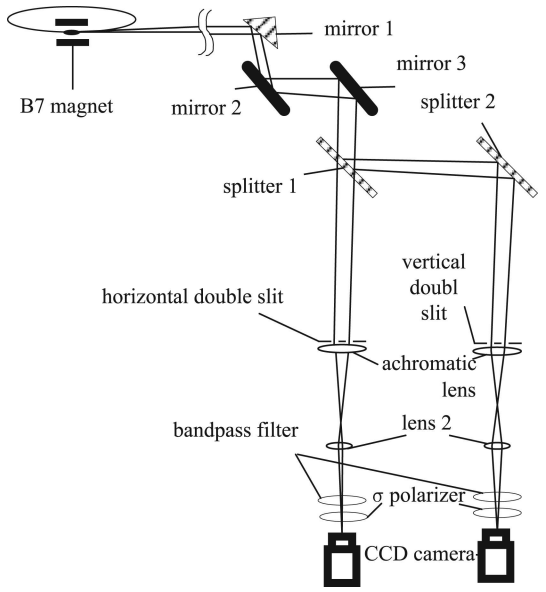

Fig. 1. Layout of the interferometer system at beamline B7.

The distance between the B7 source point and the double slit are 10.8 m for the horizontal channel and 11.1 m for the vertical channel. The slit separation is 5 mm and the size of the aperture is 0.5 mm × 2 mm (H×V) for the horizontal channel and 2 mm × 0.5 mm ($H \times V$) for the vertical channel. By adjusting the position of Lens 2 and the camera, we can magnify the pattern image by 3−5 times. The bandpass filter has a central wavelength at 500 nm and 10 nm FWHM bandwidth.

Figure 2 shows the schematic layout of the imaging system. Mirror 1 is a water-cooled oxygen-free copper. Mirrors 2–5 are reflecting mirrors. The achromatic lens has a focal length of 1400 mm. A slit (with a 21.2 mm × 21.2 mm rectangular aperture) is placed before the lens. The half-acceptance angle of the optical system limited by the slit is 3.7 mrad both in the horizontal direction and the vertical direction. After being reflected by a periscope layout (composed of mirror 4 and mirror 5), the SR is transmitted to an optical table. lens 2 is used to adjust the magnification of the imaging system.

The focal lengths of all the lenses were measured. A local bump experiment was performed to measure the magnification of the two systems. The double slit was removed for the experiment. Experiments of dispersion function measurement were achieved by changing RF. The betatron functions used were the theoretical values.

The camera has a CCD of 480 pixels × 640 pixels with pixel size of 7.4 μm × 7.4 μm. An experiment was performed to make sure that output of the CCD was linear. Experiments were also performed by analysing the image obtained by the camera at different exposure times. The results show that the beam size measurement result does not depend on the exposure time of the camera.

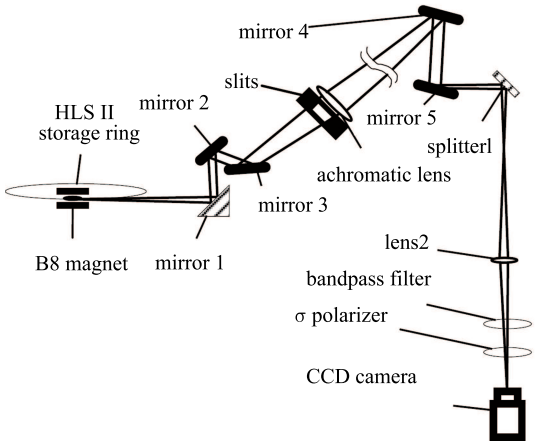

Fig. 2. Layout of the imaging system at beamline B8.

2.3 Simulation result

SRW can readily compute the SR emission [21]. The intensity distribution caused by a single electron is called the filament-beam-spread function (FBSF), and the SR intensity distribution is computed by making a 2D convolution of the FBSF with the 2D Gaussian distribution profile.

The theoretical beam size at the B7 source point is 246.9 μm(H) × 202.1 μm(V) (Table 3) and the corresponding degree of coherence is 0.3793 and 0.5201 respectively when the coupling coefficient is 10%. The degree of coherence (Table 2) can be inferred by fitting the simulated fringe with the function described in Eq. (4). The simulation γ_y is 0.5110 when the σ-polarized component of the SR is selected to illuminate the double slit, 0.5000 for the π-polarized component, and 0.5057 for total polarization. The simulation γ_y hardly depends on the polarization of the SR.

Table 2. The degree of coherence simulated by SRW using different polarization components of the SR (theoretical values are 0.3793(H) and 0.5201(V)).

parameters	σ-polarized	π-polarized	total
γ_x	0.3657	0.3656	0.3657
relative error(%)	3.56	3.61	3.56
γ_y	0.5110	0.5000	0.5057
relative error(%)	1.75	3.86	2.77

The simulated degree of coherence is less than the theoretical value (Table 1), because the wavefront used in SR was sampled at a finite area so some beam profile

information was lost. An experiment changing the sampling area size was performed. The bigger the sampled area is, the more accurate the simulation result will be.

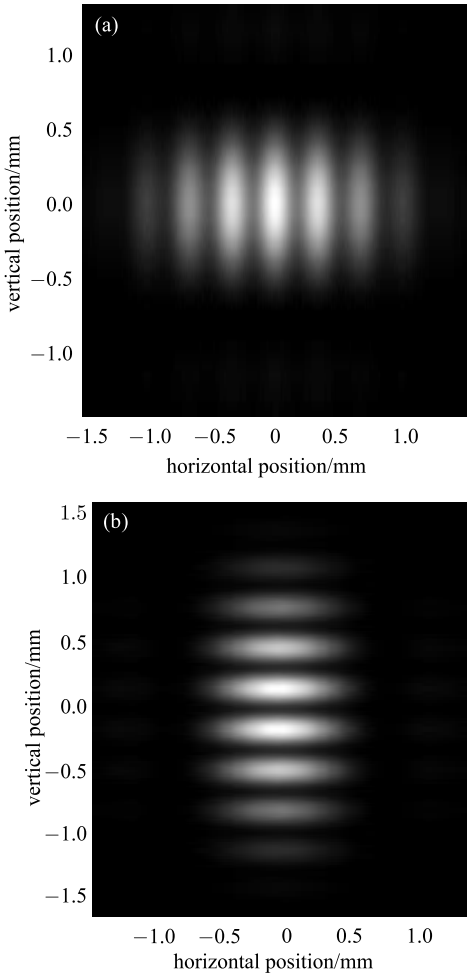

Fig. 3. The simulated (using SRW) intensity distribution of σ-polarization SR at the image plane of the interferometer system. (a) Horizontal channel assuming a finite beam ($\sigma_x = 246.9$ μm). (b) Vertical channel assuming a finite beam ($\sigma_y = 202.1$ μm).

For the imaging system, the simulation beam size is 224.1 μm (H)×163.5 μm (V) for σ-polarization, 223.3 μm (H) × 173.4 μm (V) for π-polarization and 223.9 μm (H) × 165.4 μm (V) for total polarization. The simulation error for vertical direction of the imaging system has two sources: finite size of sampling area and fitting model error. The intensity distribution of imaging with π-polarized SR is a curve which has two peaks instead of a Gaussian distribution. By comparing the simulation result with the theoretical value (218.6 μm (H)×159.5 μm (V)), we can reach the conclusion below:

1) The simulation result is in accordance with the theoretical value.

2) The simulation horizontal beam size hardly varies according to the polarization of the SR.

3) The σ-polarization of SR should be utilized to measure the vertical beam size.

Thus, we select the σ-polarization of SR to measure the transverse beam size both for the interferometer system and imaging system, both for horizontal size and vertical size.

3 Results and analysis

3.1 Measurement of beam size

In the usual operation of HLS II, coupling correction is performed with 4 skew quadrupoles in order to obtain a beam lifetime of 10 hours at 300 mA. The coupling coefficient is about 10%. Figure 4 and Fig. 5 show fringes obtained by the vertical channel and the horizontal channel respectively with a beam current of 100.4 mA.

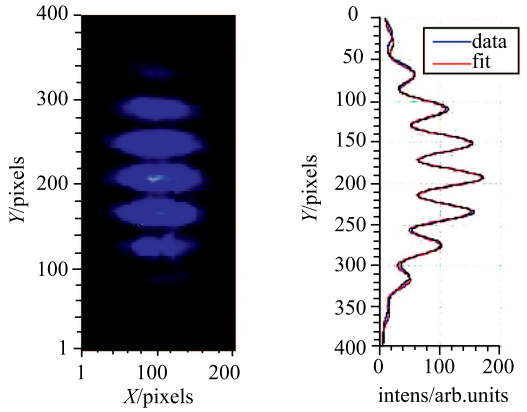

Fig. 4. A typical interference fringe obtained by the vertical interferometer using σ-polarized SR.

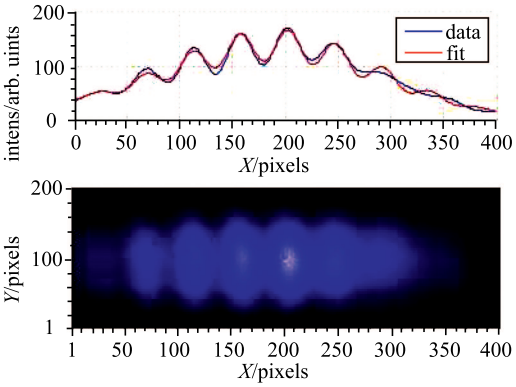

Fig. 5. A typical interference fringe obtained by the horizontal interferometer using σ-polarized SR.

The raw data is a 2D matrix with 640 rows and 480 columns. The data analysis is merely performed inside a region of interest (ROI) area. Taking the vertical beam

size analysis as an example, we set 11 columns of the matrix which are nearest to the peak position as the ROI area. By integrating the ROI along the X direction, a vector which is similar to the blue curve shown in Fig. 4 can be obtained. By fitting the curve with Eq. (1) and taking into account the imbalance between the intensities on the double slit, γ can be inferred. The measured vertical beam size is 216 μm (V) (Fig.4) and the horizontal beam size is 279 μm (Fig.5).

The vertical beam size agrees with the theoretical value (202.0 μm) at 10% coupling coefficient. The horizontal beam size is slightly larger than the theoretical value (246.9 μm). The reason might be that the real energy spread is larger than the design value.

Possible error sources of the beam size measurement by the interferometer system include imperfections in the optical components and the finite pixel size of the CCD. Besides, the error of the distance between the two slits (less than 1 μm), the slit size (less than 1 μm), the distance between the source point and the double slit (10 mm), the nonlinearity of the CCD output (1.9% uncertainty) and the non-monochromatic light (2% uncertainty) will also result in measurement error. Finally, beam jitter or camera vibration can generate a phase shift in the fringe and will reduce the visibility of the fringe [10]. Assuming the beam offset from the orbit is 50 μm, we can get a visibility error of 1.7% and a horizontal beam size error of 1.4%. The horizontal beam size measurement error due to the above causes is 3.0%.

The spatial resolution of the imaging system is constrained by the diffraction effect, the depth of field effect and the curvature error. The resolution contributed by diffraction is given by [24]

$$d_{\rm diff} = 0.5\lambda/\theta = 67.6\ \mu{\rm m}, \tag{9}$$

where θ is the half-acceptance angle of the imaging system. The depth of field error is given by [25]

$$d_{\rm dof} \approx \rho\theta^2 = 29.6\ \mu{\rm m}, \tag{10}$$

where ρ is the electron orbit radius. The curvature error is given by [26]

$$d_{\rm curv} \approx \rho\theta^2/2 = 14.8\ \mu{\rm m}. \tag{11}$$

The curvature only affects the horizontal spatial resolution. From Eq. (9), Eq. (10) and Eq. (11) we get the horizontal correction [24]

$$\Sigma_x = \sqrt{d_{\rm diff}^2 + d_{\rm dof}^2 + d_{\rm curv}^2} = 75.3\ \mu{\rm m} \tag{12}$$

and the vertical correction

$$\Sigma_y = \sqrt{d_{\rm diff}^2 + d_{\rm dof}^2} = 73.8\ \mu{\rm m}. \tag{13}$$

We can get the real beam size from the measured one by using Σ_x, Σ_y. The beam size for the B8 source point was measured during single bunch operation. A set of background images was acquired at different beam current ranges. Exposure time should change in the case of saturation or underexposure. A typical beam size measurement is 268 μm (H) × 158 μm (V) (Fig. 6) with a beam current of 0.9 mA. Measurement of beam size at different beam current was obtained (Fig. 7). 100 images were acquired at each beam current. Measurements were repeated 3 times.

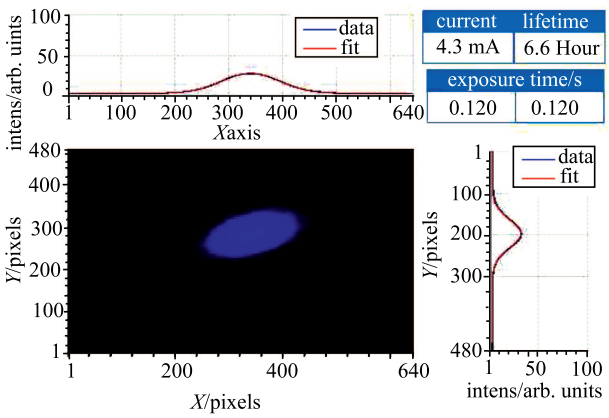

Fig. 6. The measured intensity distribution of σ-polarized SR at the image plane and the best fit. The beam current is 4.3 mA (at single bunch operation).

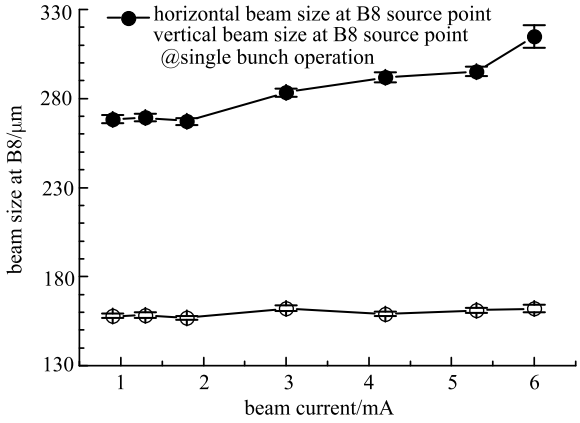

Fig. 7. The horizontal beam size and vertical beam size (±1 standard deviation) measured by the imaging system.

The vertical beam size (158 μm) agrees with the theoretical value (Table 3) and does not depend on the beam current, but the horizontal beam size is far larger than the theoretical value and depends on the beam current. It was found in the measurement that the beam became unstable when the beam current was more than 8 mA.

Table 3. The calculated and measured beam size.

methods	calculated beam size/μm	measured beam size/μm
imaging	218.6 × 159.5	268 × 158
interferometer	246.9 × 202.1	279 × 216

3.2 Measuring beam energy spread and beam emittance

Horizontal beam sizes of the B7 and B8 source points were measured simultaneously at different beam currents (from 80 mA to 240 mA with a step size of 20 mA) during multi-bunch operation (Fig. 8). The degree of coherence will be less than 0.2 and the horizontal beam size measurement error will be very large when the beam current is larger than 240 mA.

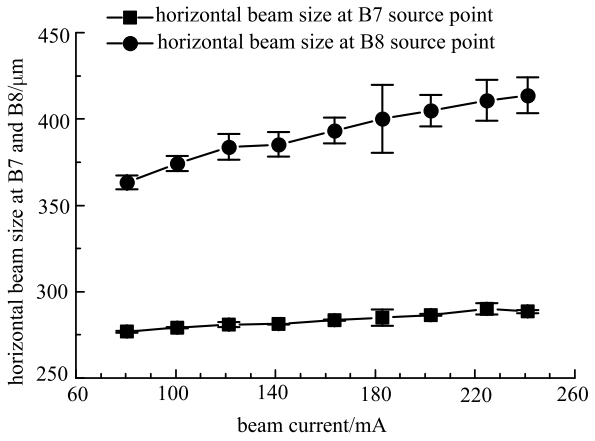

Fig. 8. The horizontal beam size (±1 standard deviation) of the B7 source point measured by the interferometer and of the B8 source point measured by the imaging system (during multi-bunch operation).

The measured horizontal beam sizes of the B7 and B8 source points are far larger than the theoretical values. From Section 3.2, the measured energy spread is larger than the theoretical value (4.7×10^{-4}). Besides, the horizontal beam size would be widened in the presence of a beam instability. From the performance of the feedback system of HLS II, we know that the transverse beam instability is reduced perfectly while the longitudinal beam instability is not reduced completely.

Statistics of the horizontal beam size of the B8 source point (at 120 mA) show that the standard deviation is 7.5 μm and the range (maximum - minimum) is 35 μm. Similarly, statistics of B7 show that the standard deviation is 1.5 μm and the range is 4 μm. Thus, the result of B8 has a larger jitter than B7.

The corresponding horizontal beam emittance and the beam energy spread are inferred (Fig. 9). The horizontal beam emittance at 220 mA is obviously an outlier (36.20 nm·rad). The rest of the points give a mean value of 35.09 ± 0.23 nm·rad. The relative beam energy spread has a positive correlation with the beam current (from 80 mA to 240 mA).

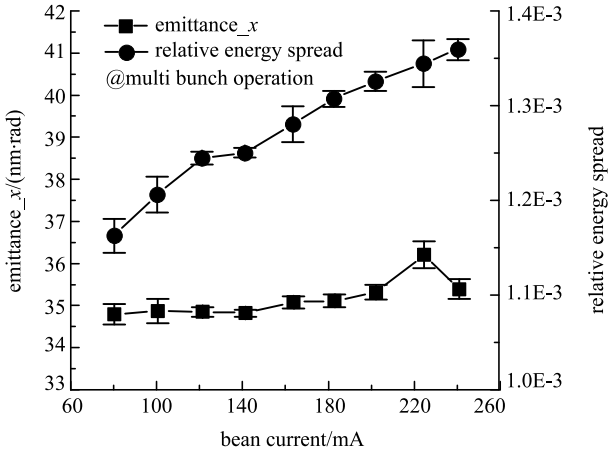

Fig. 9. Horizontal emittance and beam relative energy spread (±1 standard deviation) measured by the interferometer system and the imaging system (during multi-bunch operation).

In order to precisely measure the beam size when the beam current is more than 240 mA, a new double slit with less separation will be utilized. The longitudinal beam feedback system should also be optimized to make sure that the beam is stable.

4 Conclusion

Two transverse beam profile measurement systems using visible SR have been installed at the HLS II storage ring. One is a SR interferometer system consisting of two channels. The other is a simple imaging system which can monitor the beam transverse profile directly. Oxygen-free copper mirrors are applied to prevent thermal deformations from the SR heat load.

Simulations of these two optical systems were done using SRW. The simulation results are consistent with the theoretical values, and the σ-polarized component of SR can be used in measurement.

Measurement of beam size at different beam currents in single bunch operation have been obtained. The vertical beam size agrees with the theoretical value at 10% coupling coefficient and the horizontal beam size is larger than the theoretical value. By combining the interferometer system and imaging system, the horizontal beam emittance and the beam energy spread are inferred.

References

1 G. Kube, Review of Synchrotron Radiation based Diagnostics for Transverse Profile Measurements. in *Proceedings of the 8th European Workshop on Beam Diagnostics and Instrumentation for Particle Accelerators*, edited by I. Andrian and V. R. Schaa (Venice: DIPAC'07 EPS-AG, 2007), p. 6

2 S. Takano, Beam Diagnostics with Synchrotron Radiation in Light Sources, in *Proceedings of 1th International Particle Accelerator Conference 2010*, edited by K. Nigorikawa and A. Shirakawa (Kyoto: IPAC'10 OC/ACFA, 2010), p. 2392

3 T.Naito, T. Mitsuhashi, Improvement of the Resolution of SR Interferometer at KEK-ATF Damping Ring, in *Proceedings of 1th International Particle Accelerator Conference 2010*, edited by K. Nigorikawa and A. Shirakawa (Kyoto: IPAC'10 OC/ACFA, 2010), p. 972

4 L. L. Tang, *Development and Study of Beam Profile Measurement System for HLS II*, PhD thesis, (Hefei: University of Science and Technology of China, USTC, 2013) (in Chinese)

5 T. Mitsuhashi, Spatial Coherency of the Synchrotron Radiation at the Visible Light Region and Its Application for the Electron Beam Profile Measurement, in *Proceeding of the 17th Particle Accelerator Conference* (Vancouver, B.C: PAC'97 IEEE, 1997), p. 766

6 T. Mitsuhashi and T. Naito, Measurement of Beam size at the ATF Damping Ring with the SR Interferometer, in *Proceeding of 6th European Particle Accelerator Conference*, edited by S. Myers and L. Liljeby (Stockholm: EPAC'98 IPP, 1998), p. 1565

7 T. Mitsuhashi, Measurement of Small Transverse Beam Size Using Interferometry, in *Proceedings of the 5th European Workshop on Beam Diagnostics and Instrumentation for Particle Accelerators*, edited by K. Scheidt (Grenoble: DIPAC'01 EPS-AG, 2001), p. 26

8 T. Mitsuhashi, Twelve Years of SR Monitor Development at KEK, in *Proceedings of the 11th Beam Instrumentation Workshop*, edited by T. Shea and R. C. SiblyS (Oak Ridge: BIW'04 AIP, 2004), p. 3

9 P. Chevtsov, A. Day, and J. Denard et al, Nucl. Instrum. Methods A, **557**(1): 324 (2006)

10 J. Corbett, W. Cheng, A. Fisher et al, Interferometer Beam Size Measurements in SPEAR3, in *Proceedings of the 23rd Particle Accelerator Conference*, edited by M. Comyn (Vancouver, B. C: PAC'09 Triumf, 2009), p. 4018

11 S. T. Wang, D. L. Rubin, and J. Conway et al, Nucl. Instrum. Methods A, **703**: 80 (2013)

12 J. Chen, K. R. Ye, and Y. B. Leng, High Power Laser and Particle Beams, **23**(1): 179 (2011) (in Chinese)

13 L. L. Tang, B. G. Sun, Y. Y. Xiao et al, Nucl. Sci. Tech, **23**(4): 193, (2012)

14 Å Andersson, M. Böge, A. Lüdeke et al., Nucl. Instrum. Methods A, **591**(3): 437 (2008)

15 A. Hansson, E. Wallén, and Å Andersson, Nucl. Instrum. Methods A, **671**: 94, (2012)

16 A. S. Hernandez, N. Milas, M. Rohrer et al, The New SLS Beam Size Monitor, First Results, in *Proceedings of the 4th International Particle Accelerator Conference*, edited by Z. M. Dai and V. R. Schaa, (Shanghai: IPAC'13 JACoW, 2013), p. 759

17 L. Wang, J. X. Zhao, and J. S. Cao et al., High Power Laser and Particle Beams, **23**(9): 2512 (2011) (in Chinese)

18 M. Masaki, S. Takano, J. Synchrotron. Radiat, **10**(4): 295302 (2003)

19 T. Naito, T. Mitsuhashi, Phys. Rev. Spec. TOP-AC, **9**(12): 122802 (2006)

20 K. Tang, J. G. Wang, and B. G. Sun et al, High Power Laser and Particle Beams, **27**: 245 (2014)

21 F. Sannibale, D. Baum, N. Kelez et al, A Second Beam-Diagnostic Beamline for the Advanced Light Source, in *Proceedings of the 20rd Particle Accelerator Conference*, edited by J. Chew and P. Lucas (Portland: PAC'03 IEEE, 2003), p. 2527

22 T. Scarvie, F. Sannibale, A. Biocca et al, Beam Measurements and Upgrade at BL 7.2, the Second Diagnostics Beamline of the Advanced Light Source, in *Proceedings of the 20rd Particle Accelerator Conference*, edited by C. Horak (Knoxville: PAC'05 IEEE, 2005), p. 281

23 O. Chubar, P. Elleaume, Accurate and Efficient Computation of Synchrotron Radiation in the Near Field Region, in *Proceedings of The 6th European Particle Accelerator Conference*, edited by S. Myers and L.Liljeby (Stockholm: EPAC'98 IPP, 1998), p. 1177

24 J. A. Clarke, A Review of Optical Diagnostics Techniques for Beam Profile Measurements, in *Proceedings of The 4th European Particle Accelerator Conference*, edited by V. P. Suller and C. Petit-Jean-Genaz (London: EPAC'94 JACoW, 1994), p. 1643

25 A. Hofmann, *The physics of synchrotron radiation*, First edition (The Edinburgh Building, Cambridge: Cambridge University Press, 2004), p.230

26 J. C. Bergstrom and J. M. Vogt, Nucl. Instrum. Methods A, **562**(1): 495 (2006)